UNIVERSITY OF CALIFORNIA
SANTA CRUZ

# PRELIMINARY INVESTIGATION OF MODELS OF COUPLED CLOCKS AND COUPLED DRIVEN PENDULUMS

A thesis submitted in partial satisfaction
of the requirements for the degree of

MASTERS OF ARTS

in

MATHEMATICS

by

**Christopher A. LeBailly**

June 2013

The Thesis of Christopher A. LeBailly
is approved:

Professor Richard Montgomery, Chair

Professor Debra Lewis

Professor Jie Qing

Tyrus Miller
Vice Provost and Dean of Graduate Studies

# Table of Contents

# List of Figures

**Abstract**

Preliminary Investigation of Models of Coupled Clocks and Coupled Driven Pendulums

by

Christopher A. LeBailly

Insert abstract.

# Chapter 1

# Introduction

The Dutch mathematician and physicist Christian Huygens, who is credited with inventing the pendulum clock in 1656, made the startling observation that two pendulum clocks on a common support would synchronize over time. He described this phenomena in a letter he wrote to his farther in 1665, which is partially quoted below ([3], pgs. 153-154)

> While I was forced to stay in bed for a few days and made observations on my two clocks of the new workshop, I noticed a wonderful effect that nobody could have thought of before. The two clocks, while hanging [on the wall] side by side with a distance of one or two feet between, kept in pace relative to each other with a precision so high that the two pendulums always swung together, and never varied. While I admired this for some time, I finally found that this happened due to a sort of sympathy: when I made the pendulums swing at differing paces, I found that half an hour later, they always returned to synchronism and kept it constantly afterwards, as long as I let them go.

As a high school student I was interested in computer modeling. My physics teacher told me about Huygens' discovery and thought it would be an interesting to try and model this phenomena. I was also curious what would happen if the clocks were replaced by double pendulums since they exhibit chaotic behavior. I attempted to model the connecting beam as several point masses connected by springs. When I attempted this simulation it did not work. The position of the point masses grew larger and larger until the simulation ran out of memory. After unsuccessfully trying to fix it, I left this problem. In this paper I return to the same questions that intrigued me as a high schooler, however with a revised model and a few other tools on my belt.

# Chapter 2

# Modeling Techniques

## 2.1 Lagrangian Mechanics

In Newtonian mechanics we consider the forces acting on the system to find the equations of motion. However for more complicated systems this can become quite tedious. It is easier to compute the kinetic and potential energy for the conservative forces since these are scalar quantities (and forces are vectors). Using these energies we can use the Lagrangian approach to derive the equations of motion.

Let $T$ represent the kinetic energy of a system and let $V$ represent the potential energy. The Lagrangian is defined as $L := T - V$. Lagrange's equations states that

$$\frac{d}{dt}\left(\frac{\partial L}{\partial \dot{q_j}}\right) = \frac{\partial L}{\partial q_j} \tag{2.1}$$

where $\{q_j\}_{j=1}^n$ are the generalized coordinates and $\{\dot{q_j}\}_{j=1}^n$ are the generalized velocities of the system. If the system has non-conservative forces $Q_j$ (such as friction) which affect the $j^{th}$ generalized coordinate we can incorporate them into Lagrange's equation as follows:

$$\frac{d}{dt}\left(\frac{\partial L}{\partial \dot{q_j}}\right) - \frac{\partial L}{\partial q_j} = Q_j. \tag{2.2}$$

More information about Lagrangian mechanics, such as the derivation of equations 2.1 and 2.2, can be found in several sources (such as [1]).

## 2.2 Krasovskii-Lasalle Invariance Principle

We will now develop some machinery to determine the stability of some of the systems we will study. We follow the definitions and theorems given in [2]. A continuous

function $V(x)$ is *positive definite* if $V(x) > 0$ for all $x \neq 0$ and $V(0) = 0$. Similarly, a function is *negative definite* if $V(x) < 0$ for all $x \neq 0$ and $V(0) = 0$. We say that a function $V(x)$ is *positive semidefinite* if $V(x)$ can be zero at points other than $x = 0$ but otherwise $V(x)$ is strictly positive. We say $V(x)$ is *negative semidefinite* if $V(x)$ can be zero at points other than $x = 0$ but otherwise $V(x)$ is strictly negative.

Suppose we have a time-invariant system $\dot{x} = F(x)$, where $x \in \mathbb{R}^n$ and $\dot{x}$ denotes the time derivative of $x$. Let $x(t; x_0, t_0)$ denote the solution of this equation at time $t$ with the initial condition $x_0$ and $t_0$. The set $M \subset \mathbb{R}^n$ is said to be an *invariant set* if for all $y \in M$ and $t_0 \geq 0$, we have $x(t; y, t_0) \in M$ for all $t \geq t_0$.

We want to know what is happening as $t \to \infty$. As such, we say $x_e$ is (locally) *asymptotically stable* if for all $\epsilon > 0$, there exists a $\delta > 0$ such that

$$\|x(0) - x_e\| < \delta \Rightarrow \|x(t) - x_e\| < \epsilon \text{ for all } t > 0$$

and $x(t) \to x_e$ as $t \to \infty$ for $x(t)$ sufficiently close to $x_e$. Heuristically this mean that all nearby points converge to the equilibrium point.

**Theorem 1.** (Krasovskii-LaSalle Principle). Let $V : \mathbb{R}^n \to \mathbb{R}$ be a locally positive definite function such that on the compact set $\Omega_r = \{x \in \mathbb{R}^n : V(x) \leq r\}$ we have $\dot{V}$ is negative semidefinite. Define $S = \{x \in \Omega_r : \dot{V}(x) = 0\}$. As $t \to \infty$, the trajectory tends to the largest invariant subset of $S$. In particular, if $S$ contains no nontrivial invariant sets then 0 is asymptotically stable.

## 2.3 Runge-Kutta Method

Most Calculus students learn Euler's method to numerically solve differential equations. The formulate simply states that for a differential equation $\dot{y} = f(t, y)$

$$y_{n+1} = y_n + hf(t_n, y_n) \text{ and } t_{n+1} = t_n + h$$

where $h$ is the step size. While this is a useful method for educational purposes, in practice it is not very useful. This method is not as accurate as other methods using the same step size nor is it as stable as others.

For this paper we will use a fourth-order Runge-Kutta method. This method states that for the differential equation $\dot{y} = f(t, y)$

$$
\begin{aligned}
k_1 &= hf(t_n, y_n) \\
k_2 &= hf\left(t_n + \frac{h}{2}, y_n + \frac{k_1}{2}\right) \\
k_3 &= hf\left(t_n + \frac{h}{2}, y_n + \frac{k_2}{2}\right) \\
k_4 &= hf\left(t_n + h, y_n + k_3\right) \\
y_{n+1} &= y_n + \frac{k_1}{6} + \frac{k_2}{3} + \frac{k_3}{3} + \frac{k_4}{4} \\
t_{n+1} &= t_n + h
\end{aligned}
$$

where $h$ is the step size.

In this paper we will study many second order differential equations. To numerically solve them we will rewrite them into a system of first order equations. Suppose that $\ddot{y} = g(t, y, \dot{y})$. If $v = \dot{y}$, then $\dot{v} = \ddot{y} = g(t, y, \dot{y})$. This gives rise to the system

$$
\begin{aligned}
\dot{y} &= v \\
\dot{v} &= g(t, y, \dot{y})
\end{aligned}
$$

We can then apply the Runge-Kutta method to this system of equations to numerical solve the differential equation.

# Chapter 3

# Relevant Dynamical Systems

Next we will study some simple dynamical systems which will be important in the work to follow. A reader with some physics background will probably have seen these systems before and the derivation of equations of motion using Newtonian Mechanics. Here we shall derive these equations using the Lagrangian methods outlined above to help the reader grasp the use of the Lagrangian method.

## 3.1 Springs: Simple Harmonic Oscillator

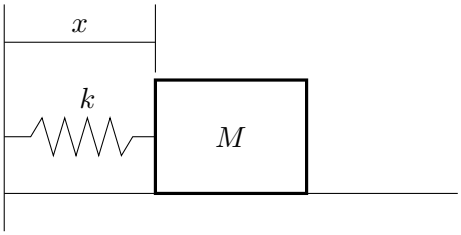


Figure 3.1: A Spring on a Frictionless Surface

We will first examine ideal springs. Hooke's law tells us that $F = -kx$ where $x$ is the displacement from the springs rest length and $k$ is the spring constant. Since $F = ma = m\ddot{x}$ we find that $\ddot{x} = -\frac{k}{m}x$. We can also arrive at this using Lagrangian Mechanics. The kinetic energy of the mass at the end of the spring is $\frac{1}{2}m\dot{x}^2$ and the potential energy stored in the spring is $\frac{1}{2}kx^2$. Hence we find that $L = \frac{1}{2}m\dot{x}^2 - \frac{1}{2}kx^2$.

Applying Lagrange's equation 2.1, we find that

$$m\ddot{x} = -kx. \tag{3.1}$$

To visualize solutions to these systems we plot the position $x$ horizontal and the velocity $\dot{x}$ vertically. Such a plot is called a *phase portrait*. Numerically integrating equation 3.1 with $k = m$ we get the phase portraits show in figure 3.2. A more realistic model accounts for

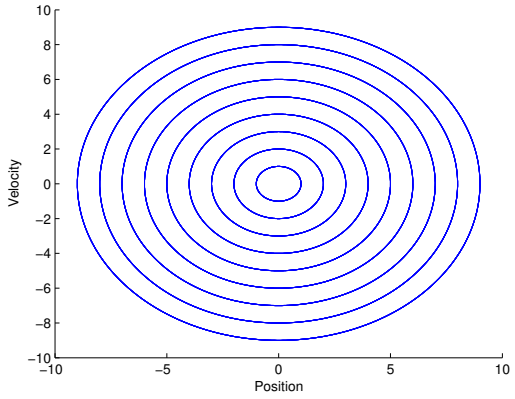


Figure 3.2: Phase Portrait for Spring

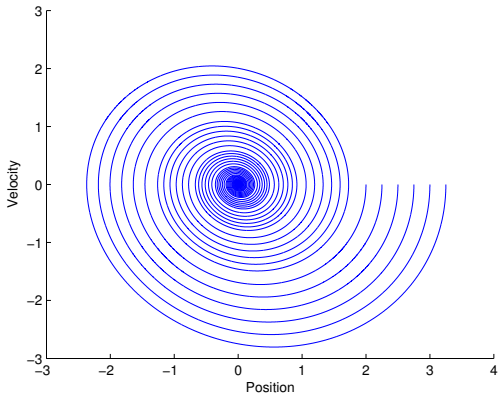


Figure 3.3: Phase Portrait for Damped Spring

friction. Applying Lagrange's equation 2.2 with $Q_x = -\mu\dot{x}$ we find that

$$m\ddot{x} + \mu\dot{x} + kx = 0. \tag{3.2}$$

Numerically integrating equation 3.2 with $k = m$ and $\mu/m = 0.2$ we get the phase portraits shown in figure 3.3.

It is clear from the phase portraits that over time all of the trajectories will tend to the origin. We can prove this using Krasovskii-LaSalle principle. To do this, consider the function

$$V = \frac{1}{2}m\dot{x}^2 + \frac{1}{2}kx^2 \tag{3.3}$$

Taking a derivative of $V$ and substituting in equation 3.2, we find $\dot{V} = m\dot{x}\ddot{x} + kx\dot{x} = m\dot{x}\ddot{x} - \dot{x}(m\ddot{x} + \mu\dot{x}) = -\mu\dot{x}$. Hence $V$ is positive-definite and $\dot{V}$ is negative semi-definite. Consider the set $S = \{(x, \dot{x}) \in \mathbb{R}^2 : \dot{V} = 0\}$. The Krasovskii-LaSalle principle tells us that any trajectory near the origin with tend towards the largest invariant subset of $S$. Since $\dot{V} = 0$ implies that $\dot{x} = 0$ we know $S = \{(x, \dot{x}) \in \mathbb{R}^2 : \dot{x} = 0\}$. For any trajectory contained in $S$ we must have $\dot{x} = 0$ identically, meaning that $\ddot{x} = 0$. Hence by 3.2, we find that $x = 0$.

Accordingly the only trajectory in $S$ is trivial, meaning the largest invariant subset of $S$ is trivial. Ergo all trajectories are asymptotically stable to the origin.

## 3.2 Pendulums

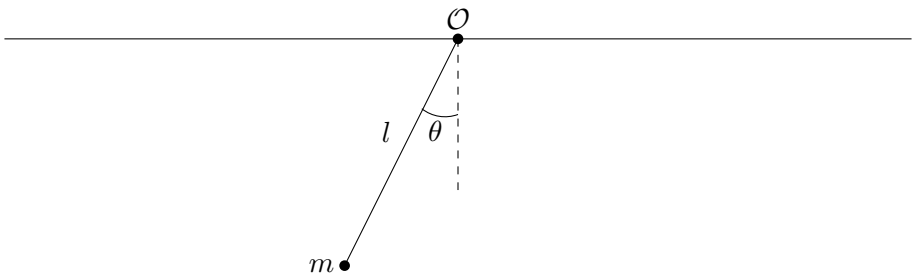


Figure 3.4: A pendulum

Consider a point with mass $m$ attached to a massless rod of length $l$ (see figure 3.4). If $x$ represents the $x$-coordinate of the mass relative to $\mathcal{O}$ and $y$ represents the $y$-coordinate of the mass relative to $\mathcal{O}$, then $x = l\sin\theta$ and $y = -l\cos\theta$. Hence

$$T = \frac{1}{2}m\big[\dot{x}^2 + \dot{y}^2\big] = \frac{1}{2}m\big[(l\dot{\theta}\cos\theta)^2 + (l\dot{\theta}\sin\theta)^2\big] = \frac{1}{2}ml^2\dot{\theta}^2$$

The potential energy is simply $V = mgy = -mgl\cos\theta$, meaning $L = T - V = \frac{1}{2}ml^2\dot{\theta}^2 + mgl\cos\theta$. Applying Lagrange's equation 2.1, we find

$$\ddot{\theta} + \frac{g}{l}\sin\theta = 0. \tag{3.4}$$

Numerically integrating equation 3.4 with $g = l$ we find the phase portrait in figure 3.5.

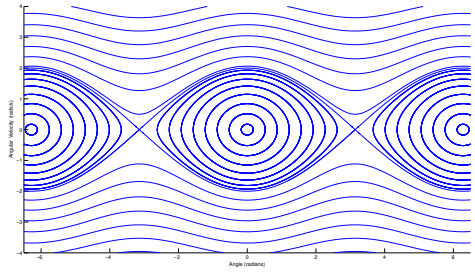

Figure 3.5: Pendulum Phase Portrait

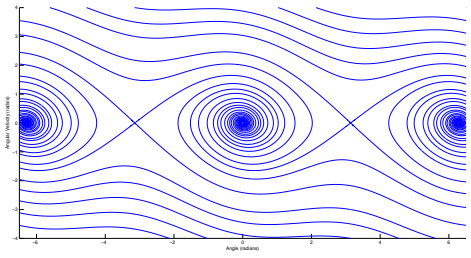

Figure 3.6: Damped Pendulum Portrait

Suppose that pendulum experiences a frictional force of $Q_\theta = -\mu\dot{\theta}$. Applying Lagrange's equation 2.2 we find

$$ml^2\ddot{\theta} + \mu\dot{\theta} + mgl\sin\theta = 0. \tag{3.5}$$

Numerically integrating equation 3.5 with $g = l$ and $\mu/ml^2 = 0.2$ we get the phase portrait in figure 3.6.

We can again see that the damped pendulum has asymptotically stable equilibrium points. To show that the origin is asymptotically stable, consider the function

$$V = \frac{1}{2}ml^2\dot{\theta}^2 + mgl(1 - \cos\theta)$$

where $\theta \in (-\pi, \pi)$. Computing the the derivative and using equation 3.5, we find $\dot{V} = ml^2\dot{\theta}\ddot{\theta} + mgl\sin\theta\dot{\theta} = -\dot{\theta}(gml\sin\theta + \mu\dot{\theta}) + mgl\sin\theta\dot{\theta} = -\mu\dot{\theta}$. Hence $V$ is locally positive-definite and $\dot{V}$ is negative semi-definite. Now consider $S = \{(\theta, \dot{\theta}) \in \mathbb{R}^2 : \dot{V} = 0\}$. We want to find the largest invariant subset of $S$. Since $\dot{V} = 0$ implies that $\dot{\theta} = 0$, we know any trajectory must have $\dot{\theta} = 0$ identically. This means that $\ddot{\theta} = 0$. Plugging this into equation 3.5, we find that $\sin\theta = 0$. Since $\theta \in (-\pi, \pi)$, we see that $\theta = 0$. Hence the only trajectory in $S$ is where $(\theta, \dot{\theta}) = (0, 0)$, which by the Krasovskii-LaSalle principle shows that the origin is asymptotically stable.

## 3.3 Clocks

Clocks clearly encounter fiction. A mechanism called an escapement supplies energy so clocks keep ticking. Following the model outlined in [5], we model the escapement as a Van der Pol oscillator. The escarpment adds an external torque $D(\theta, \dot{\theta}) = e(\gamma^2 - \theta^2)\dot{\theta}$ where $e$ is a constant which represents the strength of the escapement and $\gamma$ represents the critical angle. If $|\theta| < \gamma$ then the escapement will supply energy to the pendulum. If $|\theta| > \gamma$ the escapement will dampen the pendulum. Adding the escapement makes $Q_\theta = -\mu\dot{\theta} + e(\gamma^2 - \theta^2)\dot{\theta}$, which yields

$$\ddot{\theta} = -\frac{g}{l}\sin\theta - \frac{\mu}{ml^2}\dot{\theta} + \frac{e}{ml^2}(\gamma^2 - \theta^2)\dot{\theta}. \tag{3.6}$$

Numerically integrating equation 3.6 for four minutes we get the phase portrait in figure 3.7. If we only plot the last two minutes of the simulation we can easily see that all

initial conditions tend to the same limit cycle, shown in figure 3.8. For both simulations $g = l$, $\mu/ml^2 = 0.2$, $e/ml^2 = 1.2$, and $\gamma = 0.5$.

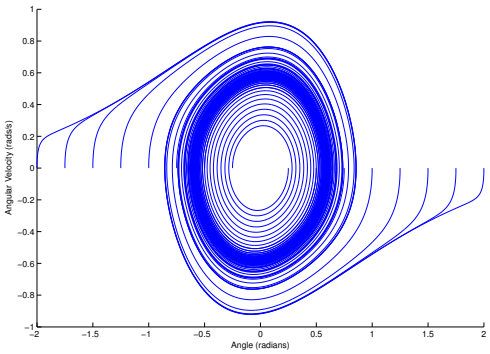


Figure 3.7: Phase Portrait for Clock

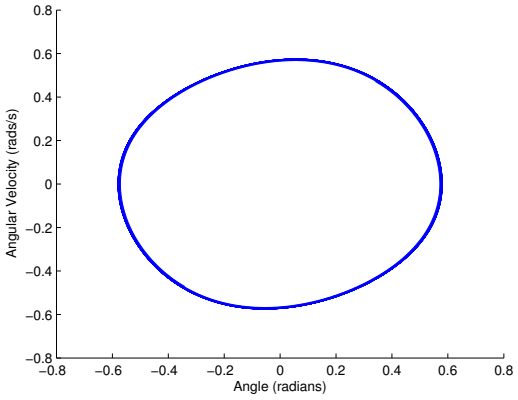


Figure 3.8: Limit Cycle for Clock

## 3.4 Driven Pendulum

The driven pendulum is similar to a normal pendulum, except that the driven pendulum is external driven by a force of $A\cos(\omega t)$, where $A$ is the forcing amplitude and $\omega$ is related to the forcing frequency. Unlike the escapement in a clock, this forcing is a function of time. While it is periodic, it may or may not coincide with the natural frequency of the pendulum. This can result in periodic, quasi-periodic, or chaotic behavior.

The Lagrangian for the driven pendulum is the same as the pendulum. Since there is a non-conservative driving forcing of $A\cos(\omega t)$ and a damping of $-\mu\dot{\theta}$, we find $Q_\theta = A\cos(\omega t) - \mu\dot{\theta}$. Using equation 2.2 we find

$$ml^2\ddot{\theta} + mgl\sin\theta + \mu\dot{\theta} = A\cos(\omega t) \tag{3.7}$$

A phase portrait for the driven pendulum is plotted in Figure 3.9, with $ml^2 = mgl = 1$, $\mu = 1/4$, $A = 3/2$, and $\omega = 2/3$. These conditions result in chaotic behavior which gives rise to a cluttered phase portrait.

One way to see more interesting features of the driven pendulum is to create a Poincare section. Imagine that we place the driven pendulum in a dark room, but turn a light on at fixed time intervals to record the pendulums angle and angular velocity. We

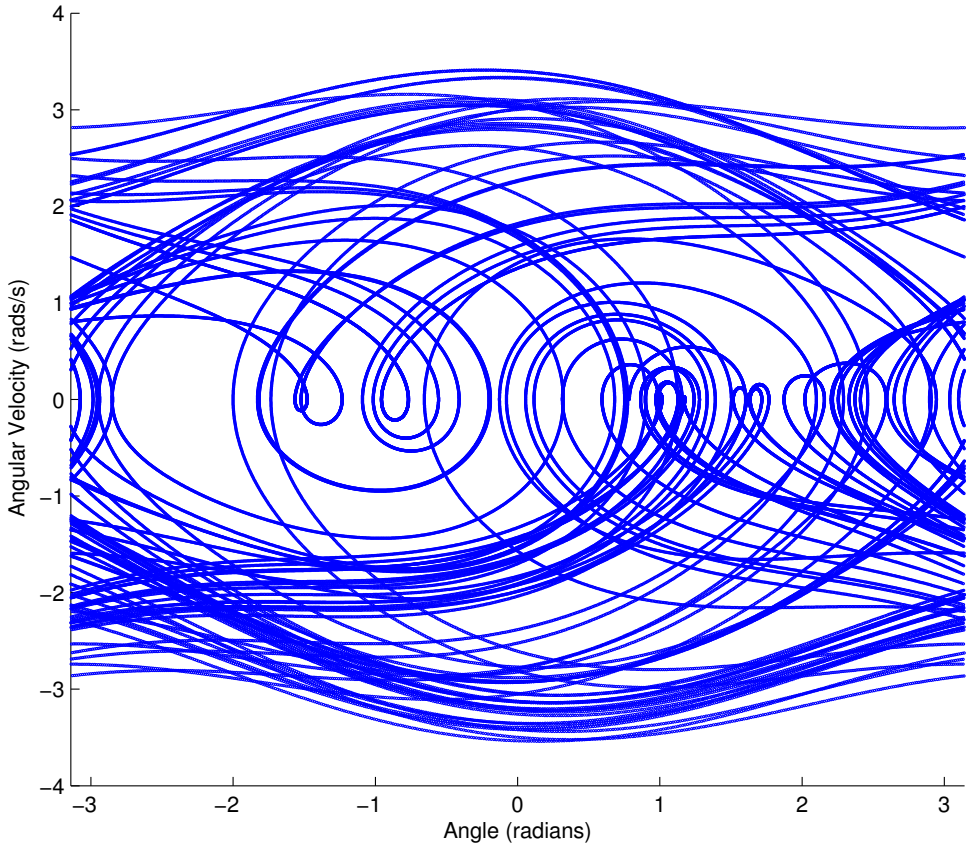


Figure 3.9: Phase Portrait for Chaotic Pendulum

can then use this data to create a phase portrait. If we strobe the pendulum at the same frequency as the driving force, we get the Poincare section pictured in figure 3.10. The reason we want to strobe at the same frequency of the driving force is to see if the motion is periodic, quasi-periodic, or chaotic. If the motion is chaotic a Poincare section like Figure 3.10, which is called a *strange attractor* of the system.

Another way to study the chaotic pendulum is through bifurcation diagrams. Suppose we fix all the parameters except for one. We still want to strobe the pendulum, but instead of plotting the angular velocity versus the angle, we just record the angular velocity. We can then plot the angular velocity vertically and the parameter we vary horizontally. When we vary the forcing coefficient we get the bifurcation diagram in Figure 3.11. When

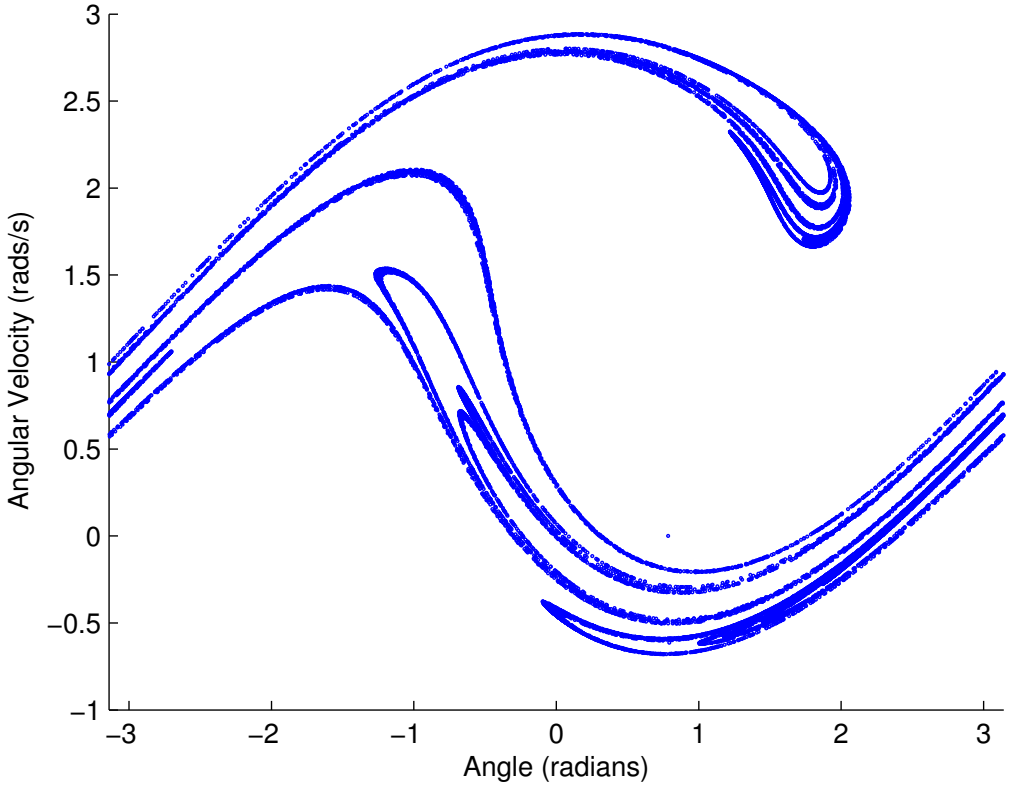


Figure 3.10: Poincare Section for Chaotic Pendulum

we vary the drive frequency we get the bifurcation diagram in Figure 3.12. When we vary the damping we get the bifurcation diagram in Figure 3.13. These diagram show us where we get different types of motion. For example, if we look at the damping bifurcation diagram, we can see for $\mu > 0.5$ that we have periodic motion. When $\mu$ is around 0.4 we get quasi-periodic motion. When $\mu < 0.1$ we get chaotic motion. We also notice that sometimes while we have chaotic motion small windows of quad-periodic motion appear. One instant of this can bet seen around $\mu = 0.14$.

## 3.5 Error in Numerical Analysis

A simple way to gauge the error committed by the Runge-Kutta algorithm is to compare the predicted theoretical energy of the system to the energy of the of the simulated system. For this method to work we need the energy to be conserved. Hence this method

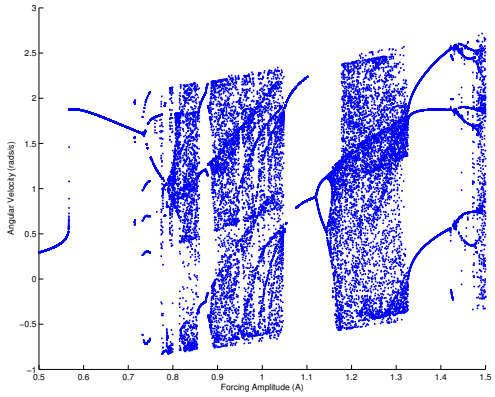


Figure 3.11: Forcing Bifurcation Diagram

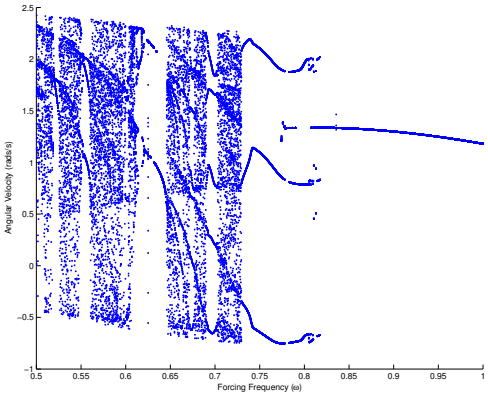


Figure 3.12: Drive Frequency Bifurcation Diagram

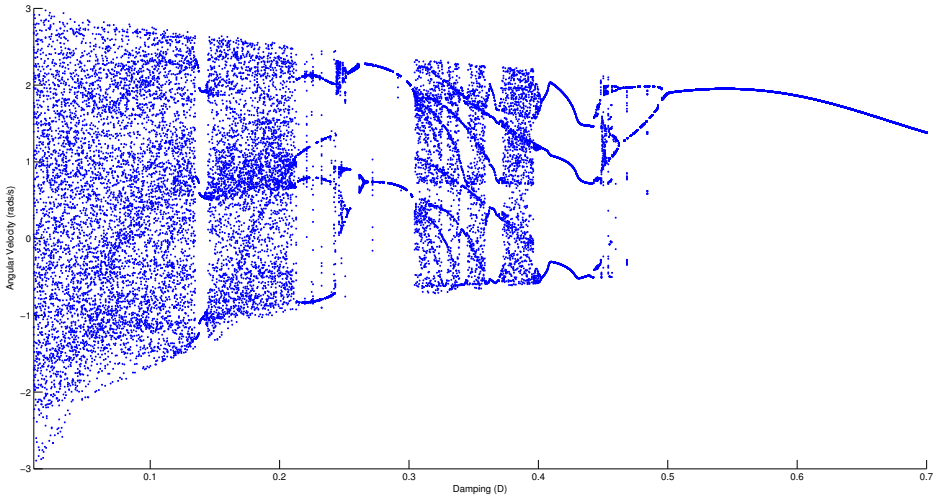


Figure 3.13: Damping Bifurcation Diagram

will only work for the frictionless spring and the frictionless pendulum, as all the other systems have non-conservative forces. Recall that relative error is given by $|E_p - E_s|/E_p$, where $E_p$ is the predicted theoretical energy and $E_s$ is the simulated energy. In figure 3.14 we show the relative error versus time for the spring with a step size of 0.01. In figure 3.15 we show the relative error for the pendulum with a step size of 0.001.

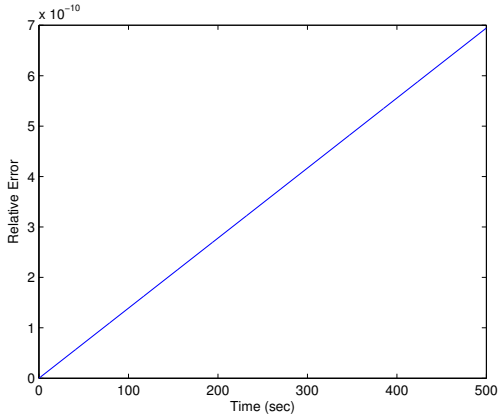


Figure 3.14: Error for Spring

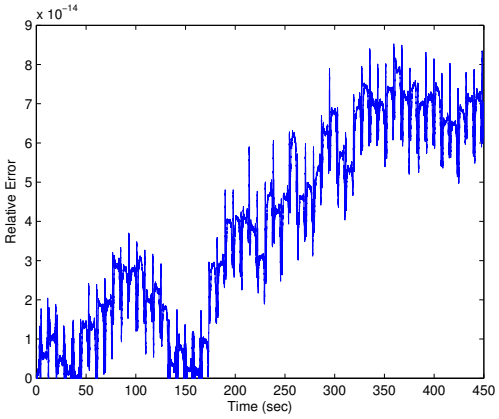


Figure 3.15: Error for Pendulum

# Chapter 4

# A Model of Two Coupled Clocks

## 4.1 Experimental Results Motivating Our Model

In [4], the authors attempted to reproduce Huygens' result experimentally. They first mounted two pendulum clocks to a walk. However they did not observed synchronization. Next they took two tables and placed a block of wood which spanned the gap between the tables. They then hung the two pendulum clocks from the beam. However they still did not observed synchronization. Next they placed two small cylindrical rollers under the beam so the beam could move back and forth. This modification made both in-phase and out-of-phase synchronization possible. Since it was experimentally shown that this set-up causes the clocks to synchronize it will serve as the basis for our model in the next section.

## 4.2 Model and Equations of Motion

In this model we will consider two pendulums with length $l$ and point mass $m$ attached at the end, affixed to a common support of mass $M$ (as shown in figure 4.2). The common support is then attached to a spring of spring constant $k$. As the common support moves it experiences damping. Suppose that the pendulums have an escapement mechanism described by $D_i = D(\theta_i, \dot{\theta}_i)$ ($i = 1$ or 2). Let $x$ measure the displacement of the support (with $x = 0$ corresponding to the spring at its rest length), and let $\alpha$ and $\beta$ be fixed distances with $\beta > 2l$ (ensuring that the pendulums never collide).

If $x_l$ represents the $x$-coordinate of the left pendulum relative to $\mathcal{O}$ and $y_l$ represents the $y$-coordinate of the left pendulum relative to $\mathcal{O}$, then $x_l = x + \alpha + l\sin\theta_1$ and $y_l =$

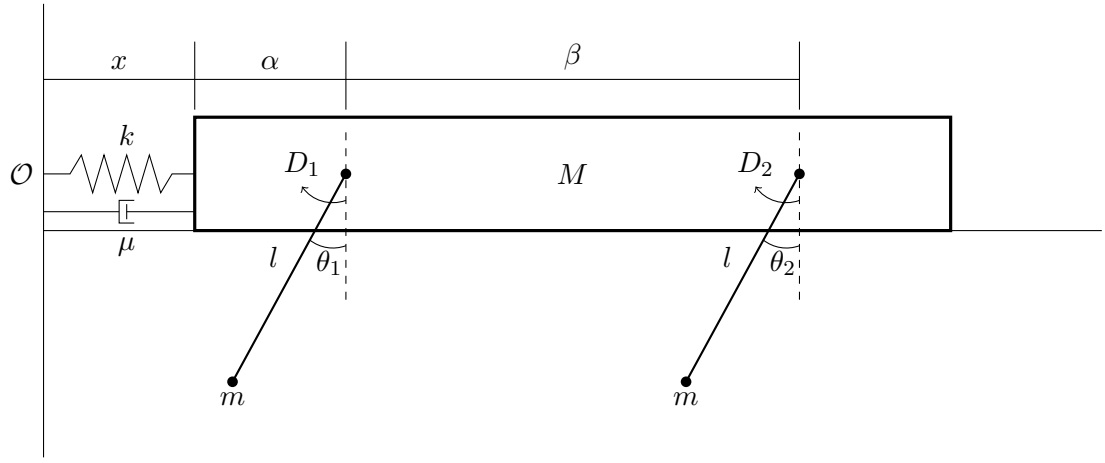


Figure 4.1: Two Pendulums on a Moving Support, attached to a damped spring

$-l\cos\theta_1$. Hence the kinetic energy from the left pendulum is

$$T_l = \frac{1}{2}m(\dot{x_l}^2 + \dot{y_l}^2) = \frac{1}{2}m\big[(\dot{x} + l\dot{\theta_1}\cos\theta_1)^2 + (l\dot{\theta_1}\sin\theta_1)^2\big].$$

Similarly if $x_r$ represents the $x$-coordinate of the right pendulum relative to $\mathcal{O}$ and $y_r$ represents the $y$-coordinate of the right pendulum relative to $\mathcal{O}$, then $x_l = x+\alpha+\beta+l\sin\theta_2$ and $y_l = -l\cos\theta_2$. Hence the kinetic energy from the right pendulum is

$$T_r = \frac{1}{2}m(\dot{x_r}^2 + \dot{y_r}^2) = \frac{1}{2}m\big[(\dot{x} + l\dot{\theta_2}\cos\theta_2)^2 + (l\dot{\theta_2}\sin\theta_2)^2\big].$$

Since the kinetic energy of the support is simply $\frac{1}{2}M\dot{x}^2$ we find the total kinetic energy is

$$T = \frac{1}{2}(M+2m)\dot{x}^2 + ml\dot{x}\big[\dot{\theta_1}\cos\theta_1 + \dot{\theta_2}\cos\theta_2\big] + \frac{1}{2}ml^2\big[\dot{\theta_1}^2 + \dot{\theta_2}^2\big].$$

The potential energy is simply the sum of the energy stored in the spring plus the gravitation potential of the two pendulums, which is

$$V = \frac{1}{2}kx^2 + mgy_l + mgy_r = \frac{1}{2}kx^2 - mgl\cos\theta_1 - mgl\cos\theta_2.$$

Hence we find the Lagrangian of the system is

$$L = \frac{1}{2}\big(M+2m\big)\dot{x}^2 + ml\dot{x}\big[\dot{\theta_1}\cos\theta_1 + \dot{\theta_2}\cos\theta_2\big] + \frac{1}{2}ml^2\big[\dot{\theta_1}^2 + \dot{\theta_2}^2\big] - \frac{1}{2}kx^2 + mgl\cos\theta_1 + mgl\cos\theta_2.$$

Since not all the forces are conservative, we must use Langrange's equation 2.2. The friction in the frame is incorporated with $Q_x = -\mu\dot{x}$, the escapement for the left

pendulum is incorporated with $Q_{\theta_1} = D_1 = e(\gamma^2 - \theta_1^2)\dot{\theta}_1$ and similarly the escapement for the right pendulum is incorporated with $Q_{\theta_2} = D_2 = e(\gamma^2 - \theta_2^2)\dot{\theta}_2$. Applying Lagrange's equation 2.2 with the three generalized coordinates $x, \theta_1, \theta_2$ yields

$$\begin{cases} gml\sin\theta_1 + ml\ddot{x}\cos\theta_1 + ml^2\ddot{\theta}_1 &= e(\gamma^2 - \theta_1^2)\dot{\theta}_1 \\ gml\sin\theta_2 + ml\ddot{x}\cos\theta_2 + ml^2\ddot{\theta}_2 &= e(\gamma^2 - \theta_2^2)\dot{\theta}_2 \\ (M+2m)\ddot{x} + kx + \mu\dot{x} + ml\big[\ddot{\theta}_1\cos\theta_1 + \ddot{\theta}_2\cos\theta_2\big] &= ml\big[\dot{\theta_1}^2\sin\theta_1 + \dot{\theta_2}^2\sin\theta_2\big] \end{cases} \tag{4.1}$$

## 4.3 Asymptotic Stability with Krasovskii-LaSalle

Following in ideas in [5] we can show a simplified version of equation 4.1 tend to an out-of-phase synchronization (we don't use same variables as [5] does). When we use the Krasovskii-LaSalle principle, we want to define our coordinates such that origin is the asymptotically stable point. Since we are interested in showing that trajectories tend towards out-of-phase synchronization, we want to introduce the variable $\theta = \theta_1 + \theta_2$. Doing so means out-of-phase synchronization will be achieved when $\theta = \dot{\theta} = 0$. However we can not do much with this in equation 4.1. We can simplify equation 4.1 by linearizing the trigonometric functions and dropping the squared terms. After doing this we can add the first two equations in 4.1 to get $\theta$. Doing so yields

$$gml\theta + 2ml\ddot{x} + ml^2\ddot{\theta} = 0 \tag{4.2}$$

$$(M+2m)\ddot{x} + kx + \mu\dot{x} + ml\ddot{\theta} = 0 \tag{4.3}$$

Consider the function

$$V = mgl\theta^2 + 2klx^2 + 2M\dot{x}^2 + m(l\dot{\theta} + 2\dot{x})^2 \tag{4.4}$$

It is clear that $V$ is a positive-definite function. Differentiating $V$ and using equations 4.2 and 4.3, we find

$$\begin{aligned}
\dot{V} &= 2mgl\theta\dot{\theta} + 2ml^2\dot{\theta}\ddot{\theta} + 4kx\dot{x} + 4M\dot{x}\ddot{x} + 8m\dot{x}\ddot{x} + 4ml[\ddot{\theta}\dot{x} + \dot{\theta}\ddot{x}] \\
&= 2\dot{\theta}(mgl\theta + ml^2\ddot{\theta}) + 4kx\dot{x} + 4(M+2m)\dot{x}\ddot{x} + 4ml[\ddot{\theta}\dot{x} + \dot{\theta}\ddot{x}] \\
&= 2\dot{\theta}(mgl\theta + ml^2\ddot{\theta}) + 4\dot{x}[kx + (M+2m)\ddot{x}] + 4ml\ddot{\theta}\dot{x} + 4ml\dot{\theta}\ddot{x} \\
&= 2\dot{\theta}(-2ml\ddot{x}) + 4\dot{x}[-\mu\dot{x} - ml\ddot{\theta}] + 4ml\ddot{\theta}\dot{x} + 4ml\dot{\theta}\ddot{x} \\
&= -4ml\dot{\theta}\ddot{x} - 4\mu\dot{x}^2 - 4ml\dot{x}\ddot{\theta} + 4ml\ddot{\theta}\dot{x} + 4ml\dot{\theta}\ddot{x} \\
&= -4\mu\dot{x}^2
\end{aligned}$$

Hence $\dot{V}$ is negative semi-definite.

Let $S = \{(\theta, \dot{\theta}, x, \dot{x}) \in \mathbb{R}^4 : \dot{V}(\theta, \dot{\theta}, x, \dot{x}) = 0\}$. The Krasovskii-LaSalle Principle tells us that any trajectory tends to the largest invariant subset of $S$. Since $\dot{V} = -4\mu\dot{x}^2$, $\dot{V} = 0$ implies that $\dot{x} = 0$. Since we are only interested in trajectories which are contained entirely within $S$, we know $\dot{x}$ must be identically zero which means that $\ddot{x} = 0$ and $x$ is a constant. Applying this to equation 4.3 we see that $kx + ml\ddot{\theta} = 0$ which means

$$\ddot{\theta} = -\frac{kx}{ml} = \text{constant}.$$

Applying this to equation 4.2 we find that $gml\theta - lkx = 0$ which means that

$$\theta = \frac{kx}{gm} = \text{constant}.$$

This means that $\dot{\theta} = \ddot{\theta} = 0$. Since $\ddot{\theta} = \ddot{x} = 0$, equation 4.2 tells us that $\theta = 0$. Hence the only invariant subset of $S$ is $(\theta, \dot{\theta}, x, \dot{x}) = (0, 0, 0, 0)$. Since the only invariant subset of $S$ is trivial, the Krasovskii-LaSalle Principle tells us that the origin is asymptotically stable. Since $\theta = \theta_1 + \theta_2$, this shows that for all trajectories, $\theta_1 + \theta_2$ tends to zero, which is an out-of-phase synchronization.

## 4.4 Investigation of Simulation

While the stability shown in section 4.3 is interesting in that it shows the result Huygen's observed, it does paint a complete picture. To fully understand what happens we need to return to equation 4.1. We now will turn our attention to the numerical simulations using the Runge-Kutta method outlined in section 2.3 and the Python programing language. To do this we need to solve equation 4.1 for $\ddot{x}, \ddot{\theta}_1$, and $\ddot{\theta}_2$. Doing so yields

$$\begin{aligned} \ddot{x} &= \frac{ml[\dot{\theta}_1^2 \sin\theta_1 + \dot{\theta}_2^2 \sin\theta_2] + \frac{1}{2}gm[\sin(2\theta_1)+\sin(2\theta_2)] - kx - \mu\dot{x} - \frac{1}{l}[D_1\cos\theta_1 + D_2\cos\theta_2]}{M + 2m - m\cos^2\theta_1 - m\cos^2\theta_2} \\ \ddot{\theta}_1 &= \frac{e(\gamma^2 - \theta_1^2)\dot{\theta}_1 - gml\sin\theta_1 - ml\cos\theta_1\ddot{x}}{ml^2} \\ \ddot{\theta}_2 &= \frac{e(\gamma^2 - \theta_2^2)\dot{\theta}_2 - gml\sin\theta_2 - ml\cos\theta_2\ddot{x}}{ml^2} \end{aligned} \tag{4.5}$$

For our first simulation let $M = 5, k = 0.1, \mu = 7, m = 0.1, l = 1$, and $g = 9.81$. We start with $\theta_1 = 1.3$, $\theta_2 = 1.1$ and $\dot{\theta}_1 = \dot{\theta}_2 = x = \dot{x} = 0$. Looking at a graph of the time series in figure 4.3 of each pendulum they seem to be close to an out-of-phase synchronization. If the pendulums are exactly out-of-phase then we would expect $\theta_1 + \theta_2 = 0$. Graphing $\theta_1 + \theta_2$ versus time it appears that $\theta_1 + \theta_2$ is tending towards zero, but is not identically zero, as shown in figures 4.4 and 4.5.

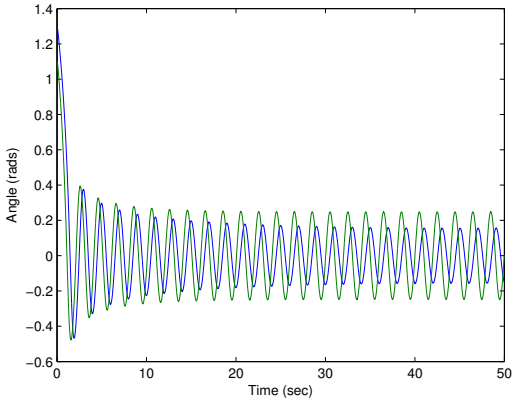


Figure 4.2: Early Time

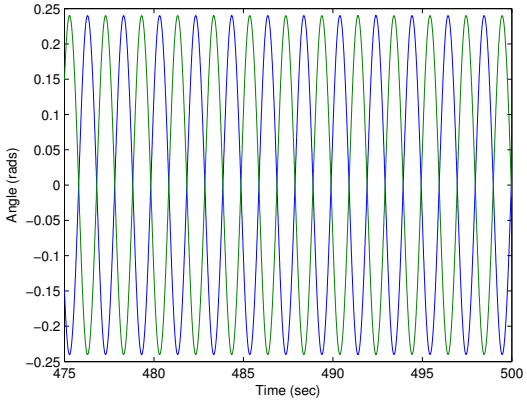


Figure 4.3: Out-of-Phase Synchronization

Now lets change the damping in the beam and let $\mu = 3$. Looking at a graph of the time series in figure 4.7 of each pendulum they seem to be close to an in-phase synchronization. If the pendulums are in-phase then we would expect $\theta_1 - \theta_2 = 0$. Graphing $\theta_1 - \theta_2$ versus time it appears that $\theta_1 - \theta_2$ is tending towards zero, but is not identically zero, as shown in figures 4.8 and 4.9.

This raises the question of how do the dynamics change as we vary the damping in the beam. We have just seen for small damping that in-phase synchronization occurs and for larger damping out-of-phase synchronization occurs. What happens as we vary the damping? How does the system transition from in-phase to out-of-phase synchronization? To study this we need to develop a criteria for when synchronization is achieved.

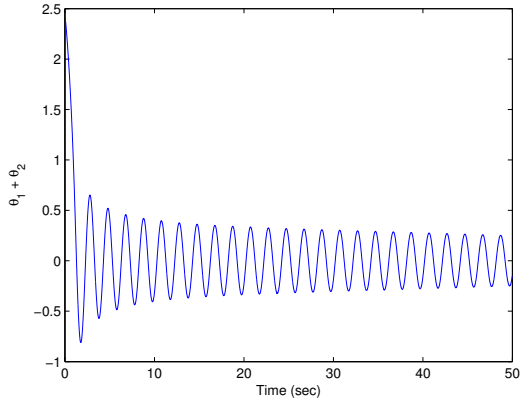


Figure 4.4: $\theta_1 + \theta_2$ for Early Time

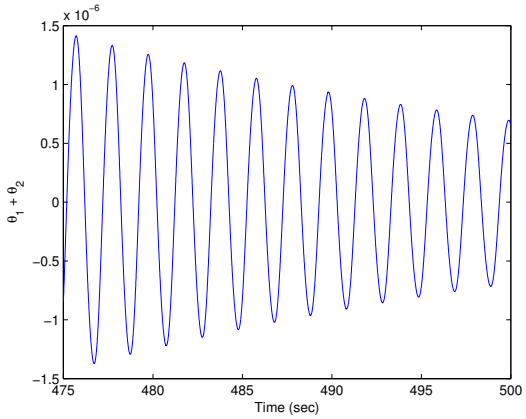


Figure 4.5: $\theta_1 + \theta_2$ when synchronized

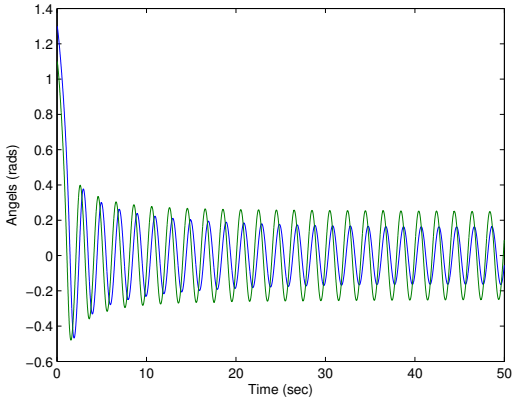


Figure 4.6: Early Time

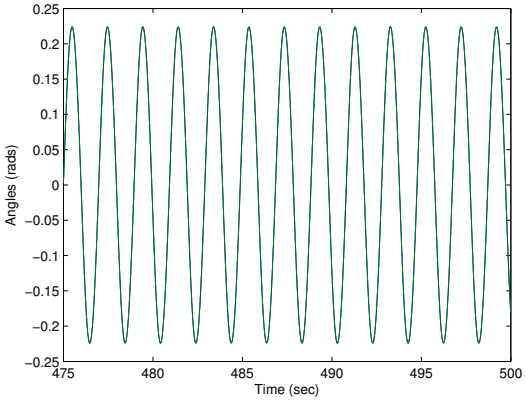


Figure 4.7: In-Phase Synchronization

The above time series graphs show that while either $\theta_1 + \theta_2$ or $\theta_1 - \theta_2$ is tending to zero, it does not become identically zero. Hence we define in-phase synchronization to mean there exists a $T$ such that $|\theta_1(t) - \theta_2(t)| < \epsilon$ for all $t > T$ (where $\epsilon$ is small). We define out-of-phase synchronization to mean there exists a $T$ such that $|\theta_1(t) + \theta_2(t)| < \epsilon$ for all $t > T$ (where $\epsilon$ is small). We will call $T$ the time when synchronization is achieved. We can write the program to find the time when synchronization is achieved as we vary $\mu$ and to classify the type of synchronization, which we show in Figure 4.10.

This pictures suggest there is a critical damping where the synchronization switched form in-phase to out-phase. We are now interested in what happens at this critical damping. In order to study it we need to find where this critical damping occurs Let $\mu_c$ be the

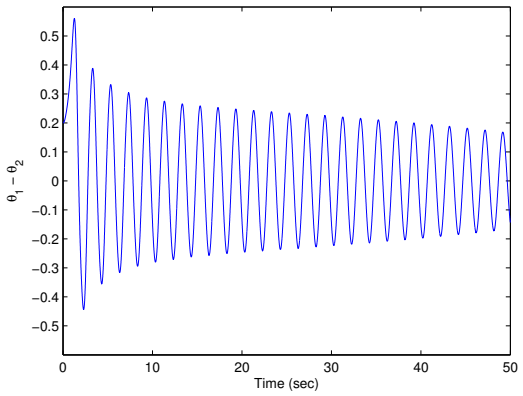


Figure 4.8: $\theta_1 - \theta_2$ for Early Time

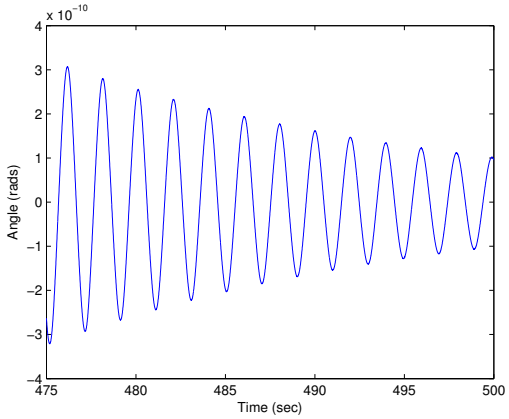


Figure 4.9: $\theta_1 - \theta_2$ when synchronized

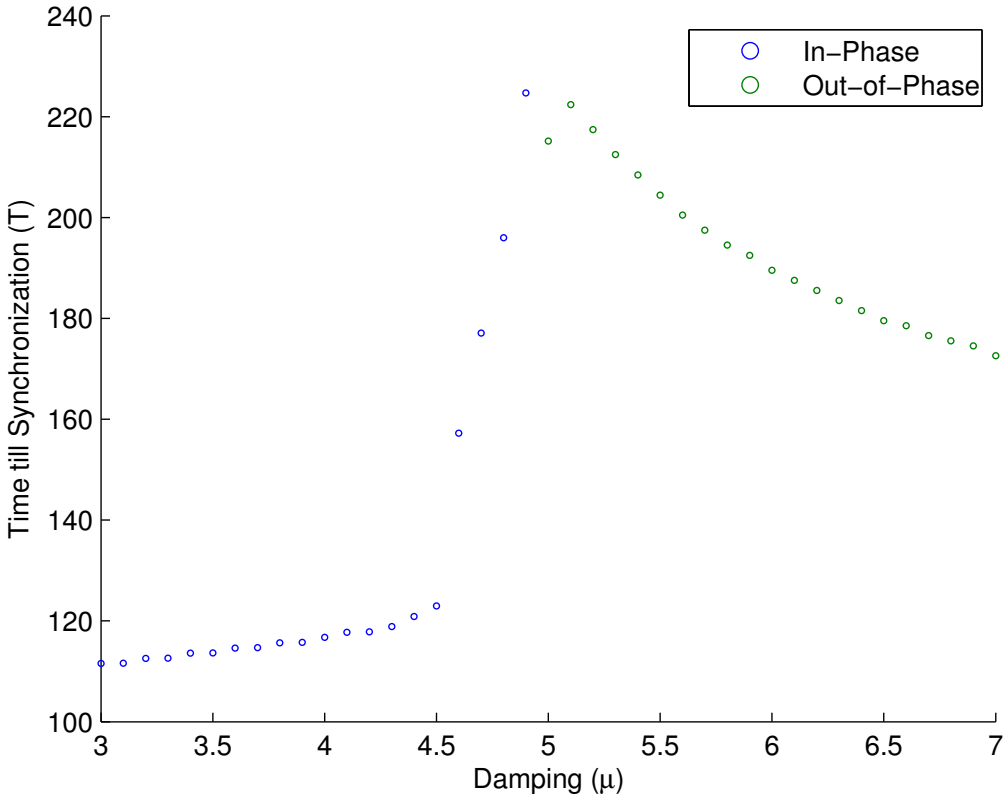


Figure 4.10: Time to Synchronize vs. Damping ($\epsilon = 0.01$)

critical damping. To estimate $\mu_c$ we will use a bisection method. We start with $\mu_{min} = 4$ which we know gives in phase synchronization and $\mu_{max} = 6$ which gives out-of-phase synchronization. We test the midpoint to see what type of synchronization occurs. If in-phase synchronization occurs we replace $\mu_{min}$ with the midpoint. If out-of-phase synchronization is achieved, then $\mu_{max}$ is replaced with the midpoint. This is repeated until neither in-phase nor out-of-phase synchronization is detected at the midpoint. It is possible that synchronization occurs at a time greater than the time the simulation ran, but we know for sure that the actual critical damping must be between $\mu_{min}$ and $\mu_{max}$. Running this we find that $4.96417299006 \leq \mu_c \leq 4.96417299029$. Figure 4.11 shows the time series where $\mu = 4.96417299018$ (the midpoint of the interval we found). As we can see that no synchronization occurs here.

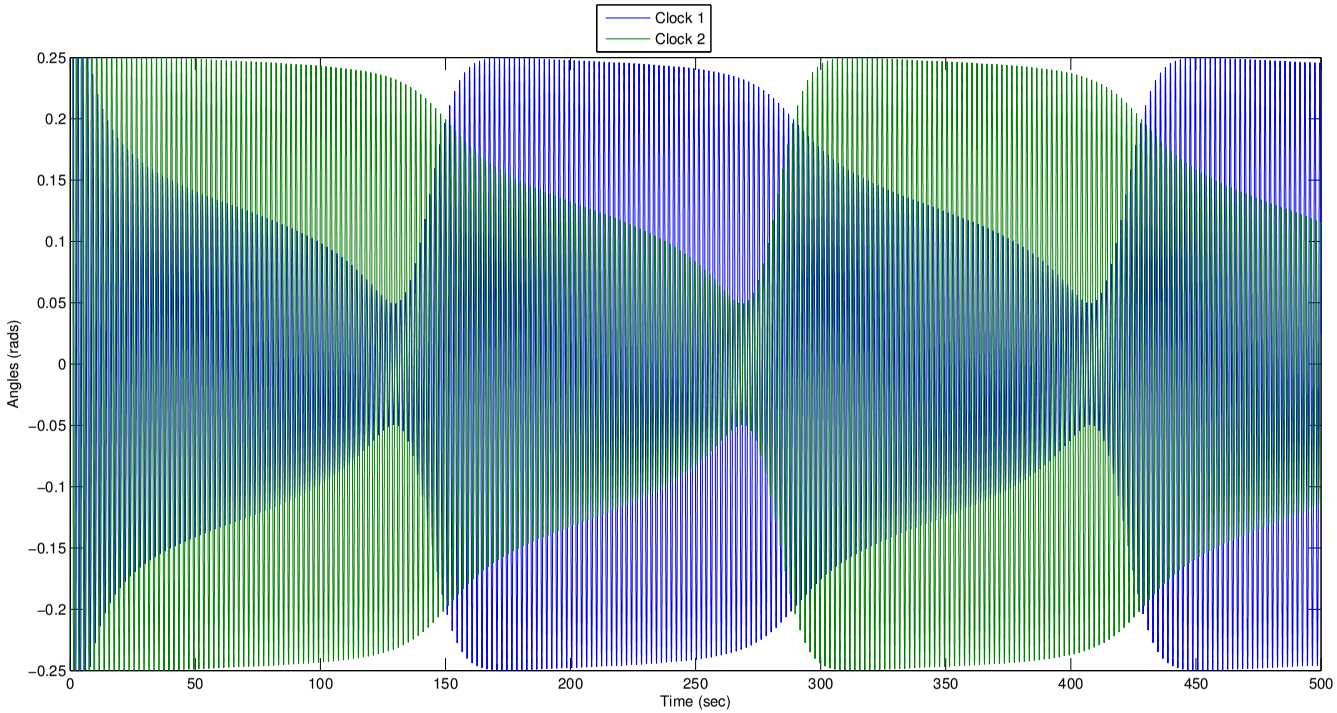


Figure 4.11: NoSynchronization at Critical Damping

# Chapter 5

# Coupled Driven Pendulums

In this section we will now make a few slight changes to the system we studied in the previous chapter. As we saw in section 3.3, adding an escapement to a pendulum causes a limit cycle to appear. This is the model we used for a clock in the previous chapter. However if we change this to the time dependent function $A\cos(\omega t)$ we have a driven pendulum which has very different behaviour. We will now look at what happens when we couple two driven pendulums.

## 5.1 Equations of Motion

The equations of motion for the coupled driven pendulums are very similar to equation 4.1. We simply need to replace the equation for the escapement with the equation for the time dependent driver. Hence $Q_{\theta_1} = Q_{\theta_2} = A\cos(\omega t)$. This yields the system

$$\begin{cases} gml\sin\theta_1 + ml\ddot{x}\cos\theta_1 + ml^2\ddot{\theta}_1 &= A\cos(\omega t) \\ gml\sin\theta_2 + ml\ddot{x}\cos\theta_2 + ml^2\ddot{\theta}_2 &= A\cos(\omega t) \\ (M+2m)\ddot{x} + kx + \mu\dot{x} + ml\big[\ddot{\theta}_1\cos\theta_1 + \ddot{\theta}_2\cos\theta_2\big] &= ml\big[\dot{\theta_1}^2\sin\theta_1 + \dot{\theta_2}^2\sin\theta_2\big] \end{cases} \tag{5.1}$$

## 5.2 Time Series

Now lets take a look at how the angel evolves over time. For these simulations we let $M = 7.5$, $k = 0.11$, $\mu = 10$, $m = 0.1$, $l = 1.0$, and $g = 9.81$. We start at $\theta_1 = 2$, $\theta_2 = -2$, and $\dot{\theta}_1 = \dot{\theta}_2 = x = \dot{x} = 0$. As we an see, there is some irregular behavior at the start but it

clearly settles down into non-chaotic behavior. Early on one of the driven pendulum make several revolutions before settling down. As such for the plot we mod out the angels by $2\pi$ to make it easier to display. This is only needed for figure 5.1. Looking at the sum $\theta_1 + \theta_2$ also helps us see what is going on, which is displayed in figures 5.1, 5.2, and 5.3.

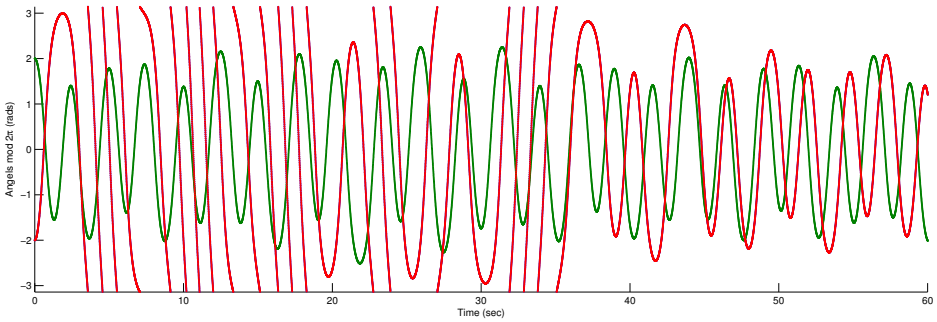


Figure 5.1: Coupled Driven Pendulums Part 1

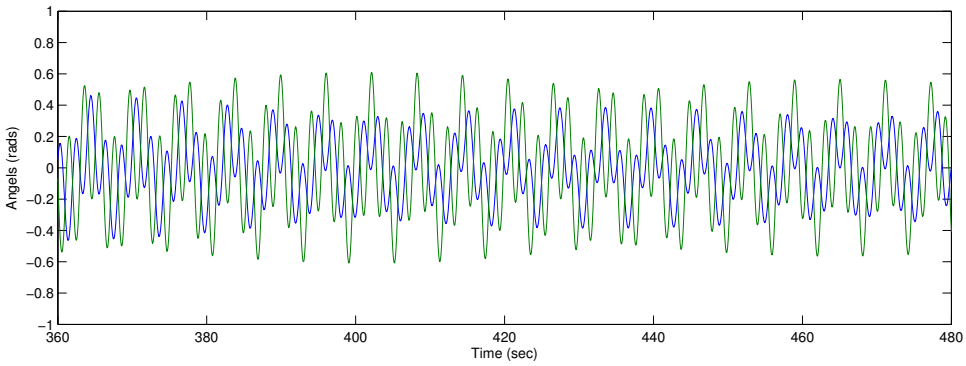


Figure 5.2: Coupled Driven Pendulums Part 2

## 5.3 Phase Portraits

Lets now look at some phase portraits for the two coupled driven pendulums. We saw before in section 3.4 that the phase portrait for the driven pendulum was very cluttered. However we see that when we look at the phase portraits, shown in figures 5.7 and 5.8, for each of the driven pendulums that they are much less cluttered.

Further more, if only look at the second half of the data, it appears that the

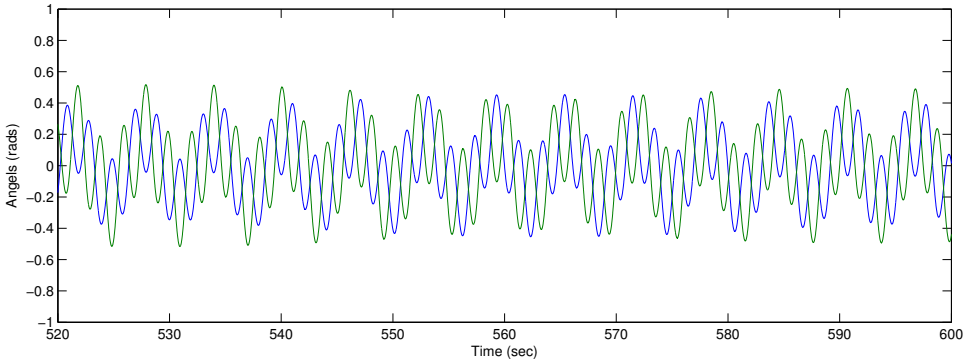


Figure 5.3: Coupled Driven Pendulums Part 3

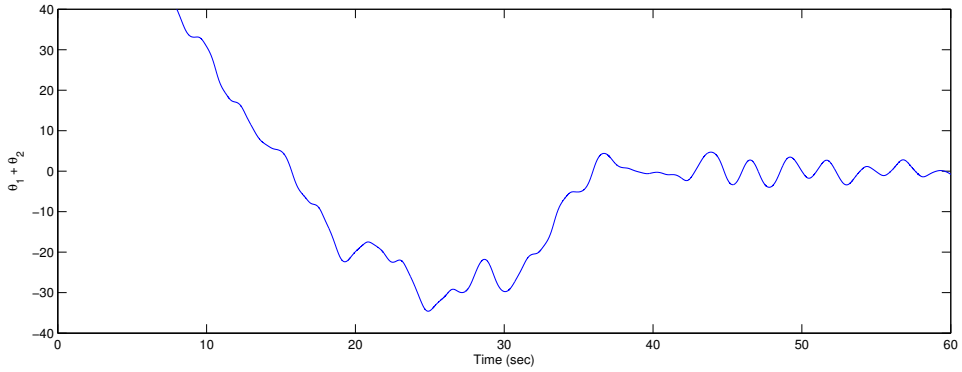


Figure 5.4: Sum of Coupled Driven Pendulums Part 1

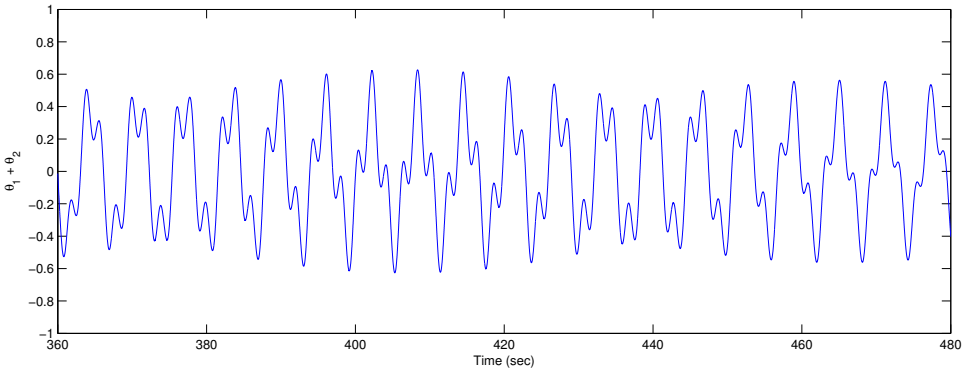


Figure 5.5: Sum of Coupled Driven Pendulums Part 2

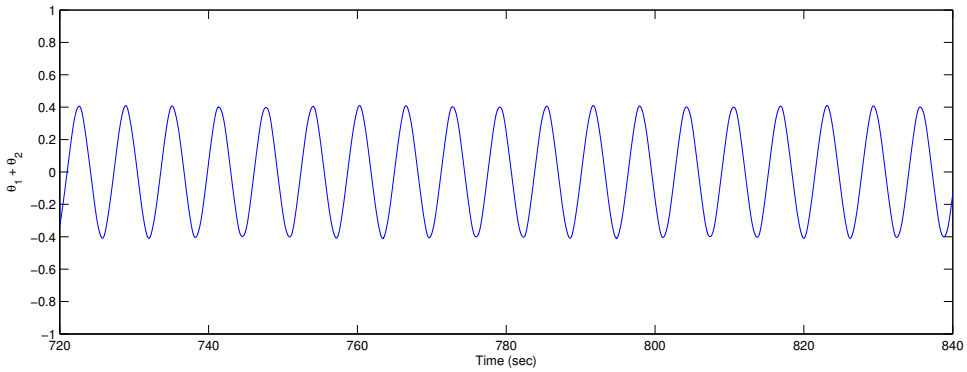


Figure 5.6: Sum of Coupled Driven Pendulums Part 3

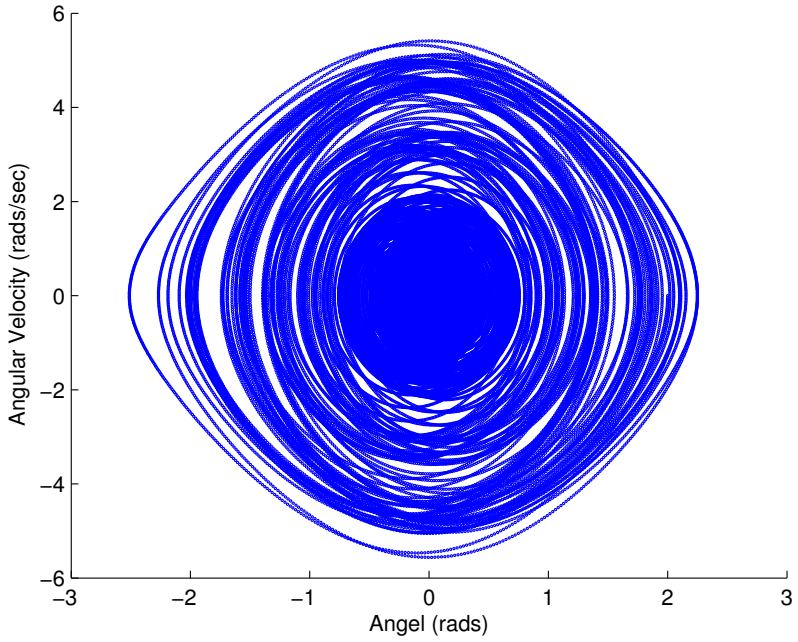


Figure 5.7: Left Pendulum Phase Portrait

behavior is no longer chaotic as shown in figures 5.9 and 5.10. This is very surprising considering the behavior we observed for the uncoupled system. Of course this is for just one set of initial conditions and system parameters. Instead of looking at tons of phase portraits, we can get the same information in a bifurcation diagram.

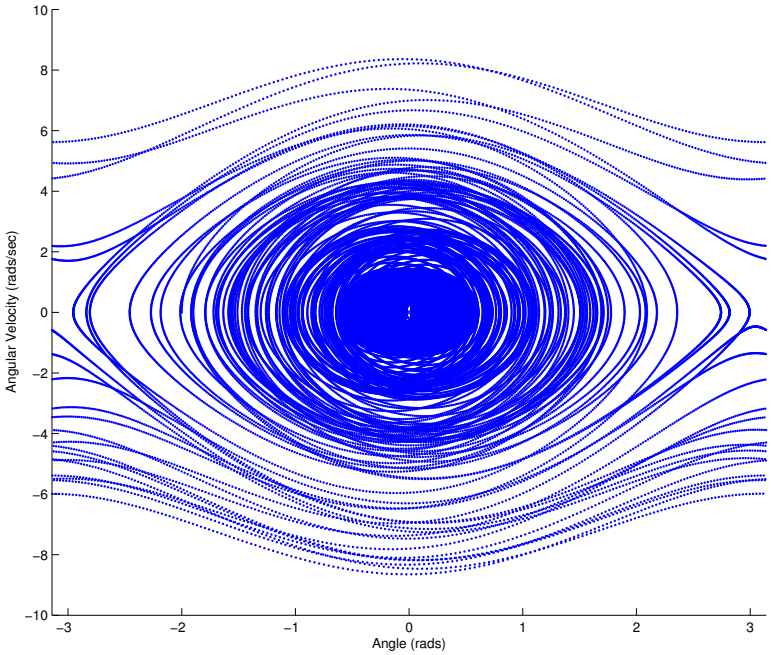


Figure 5.8: Right Pendulum Phase Portrait

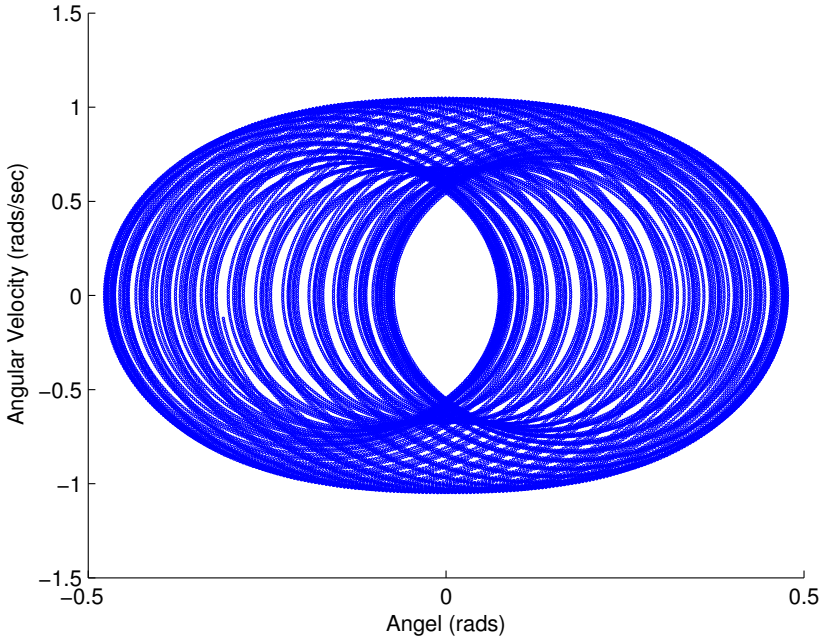


Figure 5.9: Left Pendulum Limit Cycle

## 5.4 Bifurcation Diagram

We now turn our attention to bifurcation diagrams. As we saw before in section 3.4, the bifurcation diagrams gave us an idea of when the system is chaotic and when it is periodic or quasi-periodic. The phase portraits we looked at in the previous section suggest that the motion of both pendulums settles down. As we did in section 3.4, we want to use the bifurcation diagram to see where we get periodic, quasi-periodic, or chaotic behavior. Recall that we vary one of the parameters and record the angular velocity. We strobe the angular velocity at the same frequency as the driver. The resulting bifurcation diagrams (figures 5.11 and 5.12) shows that we no longer get chaotic behavior for either driven pendulum as we vary forcing. If we vary the drive frequency (figures 5.13 and 5.14) we also don't see chaotic behavior. We do however see some chaotic behavior for small damping (figures 5.15 and 5.16).

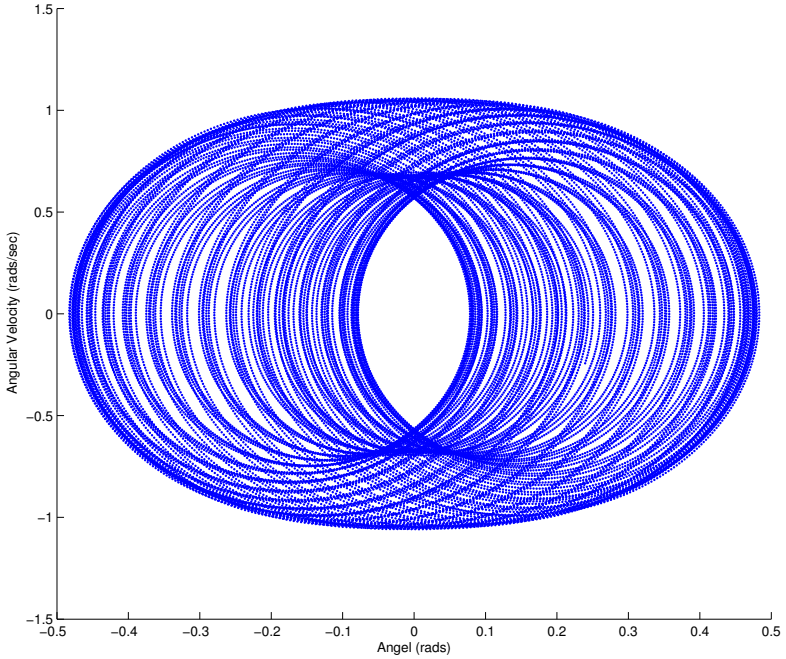


Figure 5.10: Right Pendulum Limit Cycle

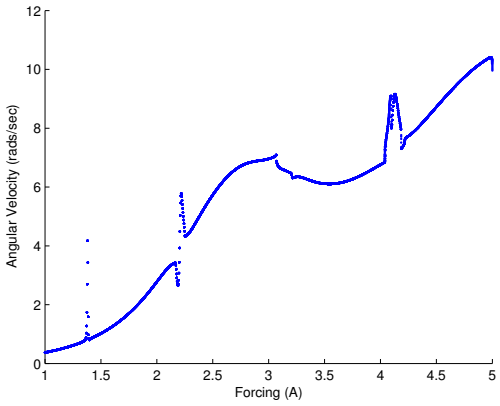


Figure 5.11: Left Forcing Bifurcation Diagram

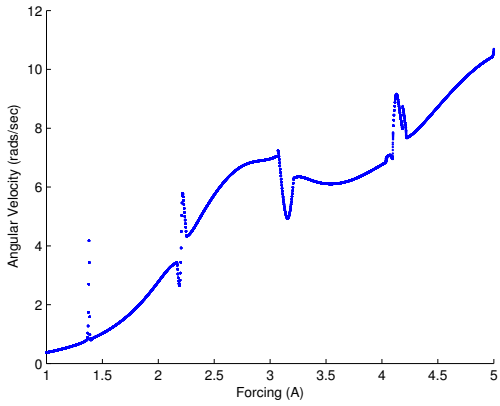


Figure 5.12: Right Forcing Bifurcation Diagram

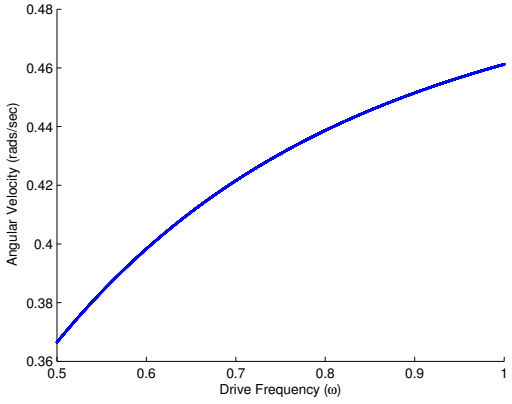


Figure 5.13: Left Drive Frequency Bifurcation Diagram

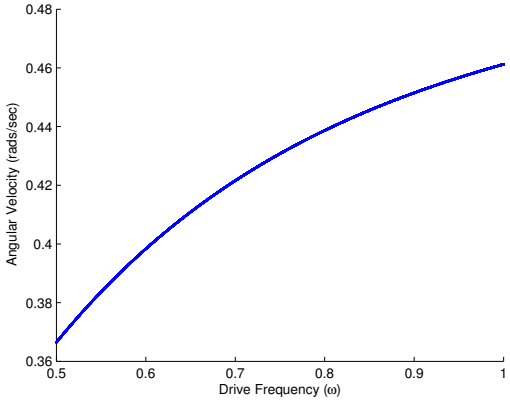


Figure 5.14: Right Drive Frequency Bifurcation Diagram

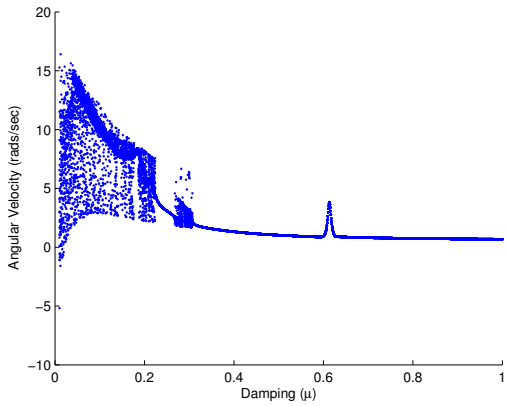


Figure 5.15: Left Damping Bifurcation Diagram

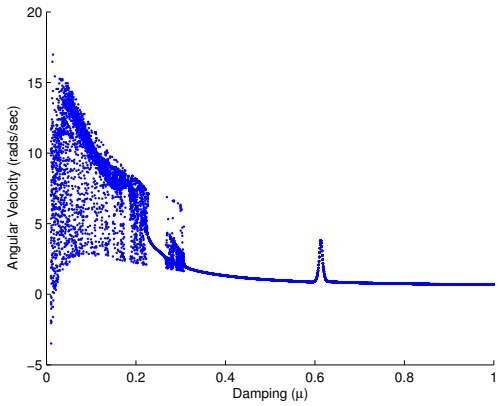


Figure 5.16: Right Damping Bifurcation Diagram

# Chapter 6

# Future Work and Conclusions

The biggest surprises encountered in this work was with the coupled driven pendulum. Seeing this coupling of two chaotic oscillators produce non-chaotic behavior was not expected. The first question raised is this an artifact of the numerical methods used or is this truly how this system behaves? If it is truly how the system behaves, why does this happen? Is there a global attractor which all initial conditions are drawn to?

We also observed an interesting phenomena when looking at the coupled clocks. As we varried the damping there was a transition from in-phase synchronization to out-of-phase synchronization. This suggests that there is a bifurcation which occurs at the critical damping. An interesting aspect would be to study the dynamics behind this bifurcation.

Another area where more work can be done is in visualizing the data. Both coupled oscillators live in a six dimensional phase space. To see our data we took various two diminutional slices to visualize the data. We could look at three dimensional slices, which could potentially yield more information. In addition to finding other ways to visualize the data we could also look at other ways to analyze the data. We primarily looked at graphs which seemed to indicated certain phenomena, but a more formal analysis would be needed to show these actually exist (and not simply an artifact of the numerical methods).

There are also a number of parameters to vary with these systems. In this paper we focused on the changes in the dynamics as we varied the damping. There are other parameters we could vary which might produce interesting results. Also we could look at for a fixed set of parameters what happens as we vary the initial conditions.

# Bibliography


[1] V. I. Arnol′d. *Mathematical methods of classical mechanics*, volume 60 of *Graduate Texts in Mathematics*. Springer-Verlag, New York, second edition, 1989. Translated from the Russian by K. Vogtmann and A. Weinstein.

[2] Karl Johan Åström and Richard M. Murray. *Feedback systems*. Princeton University Press, Princeton, NJ, 2008. An introduction for scientists and engineers.

[3] Gregory L. Baker and James A. Blackburn. *The pendulum*. Oxford University Press, Oxford, 2005. A case study in physics.

[4] K. Czolczynski, P. Perlikowski, A. Stefanski, and T. Kapitaniak. Huygens' odd sympathy experiment revisited. *International Journal of Bifurcation and Chaos*, 21(07):2047–2056, 2011.

[5] Vojin Jovanovic and Sergiy Koshkin. Synchronization of huygens' clocks and the poincaré method. *Journal of Sound and Vibration*, 331(12):2887 – 2900, 2012.

[6] William H. Press, Saul A. Teukolsky, William T. Vetterling, and Brian P. Flannery. *Numerical recipes in C*. Cambridge University Press, Cambridge, second edition, 1992. The art of scientific computing.